The Structure and Growth Process of Au/Si(111) Analyzed by High-resolution Ion Scattering Coupled with Photoelectron Spectroscopy

Y. Hoshino[1,2], Y. Kitsudo[1], M. Iwami[3], and Y. Kido[1]

Abstract

We analyzed both the elemental depth profile and chemical bonds of Au/p-Si(111)-7×7 grown at room temperature by medium energy ion scattering combined with photoelectron spectroscopy using synchrotron-radiation-light. It is found unambiguously that Au deposition grows some Au-rich silicide phases for Au coverage above 0.31 ML (1 ML = 0.78×10^{15} atoms/cm^2). At an Au coverage of 5.2 ML, the surface comprises a stable Au_3Si_2(1.5×10^{15} atoms/cm^2: ~2 atomic layers) layer on top and an underlying metallic Au layer which contains Si atoms diffused in the boundaries of fine Au grains. Indeed, we observed two components for Au 4f (Au-silicide and metallic) and three components for Si 2p spectra (bulk, Au-silicide, and incorporated in an Au layer). Further Au deposition increases thickness of the underlying Au layer without changing the thickness of the Au_3Si_2 layer on top. Total number of Si atoms consumed to form the Au_3Si_2 layer and contained in the underlying Au layer coincides with the number of Si atoms making the 7×7 reconstruction. The present study reveals clearly the dynamic process happening at the Au/Si(111) interface.

[1] *Department of Physics, Ritsumeikan University, Kusatsu, Shiga-ken 525-8577, Japan*

[2] *Department of Information Science, Kanagawa University, Hiratsuka, Kanagawa 259-1293, Japan*

[3] *Research Lab. for Surface Science, Okayama University, Okayama 700-8530, Japan*

I. INTRODUCTION

Gold (Au) is well known to be a very stable and non-reactive noble metal. However, it was found that Au is very reactive on a Si surface even at room temperature (RT)[1-4] and heating Au/Si at a low temperature of 100° C in O_2 ambience leads to formation of thick SiO_2 layers on top[5]. Recently, it was also found that gold becomes highly active as a catalyst, if its size is in scale-down to a nm range[6]. Such an intriguing property has attracted much attention in terms of the electronic properties dependent on the size and shape of gold particles[7,8]. For the Au/Si grown at RT, there are tremendous papers on the atomic and electronic structures[1-5, 9-20]. In spite of such many efforts, the phase and electronic structure together with the kinetic behavior are still debatable issues.

According to the report of Braicovich et al.[2], the Au atoms deposited at RT are dispersed in and on the Si substrate at low Au coverages and with increasing the coverage an Au-Si alloy with variable composition is formed at the Au-Si interface. Hiraki et al.[9,10] proposed a screening model that the conduction electrons in a metal overlayer screen the Coulomb interaction between substrate Si atoms, leading to the Si-Si bond breaking. Such a screening effect becomes pronounced above Au coverage of 1-5 monolayers (MLs)(critical thickness), and as a result, an Au-Si amorphous alloy is easily formed. The other structure model was reported that Au-Si intermixing takes place at an early stage of Au deposition and at higher coverages a stable Au-silicide layer is formed on a metallic Au layer[13,15,16,19]. The core level shifts of Au 4f and Si 2p observed are due to hybridization of Au and Si valence electrons. Landree et al.[17] reported growth of small poly-crystal Au domains without any Au-silicides, which was observed by a high-resolution transmission electron microscope combined with X-ray photoelectron spectroscopy (XPS). They interpreted the higher binding energy shifts of Au 4f at small Au coverages were responsible for the core hole created during photoemission so called final state effect. Recently, Kim et al.[20] analyzed Au/Si(111) and Au/Si(001) systems by positron-annihilation- and electron-induced Auger electrons spectroscopy and claimed that Au-Si intermixing took place with variable composition at Au coverage from 0.5 to 3 ML and an $Au/Au_xSi_{1-x}/Si$ structure was formed at Au coverage above 3 ML.

As mentioned above, general consensus is not yet obtained for the phases and electronic structures of the Au/Si formed at RT. In this study, we analyze both the elemental compositions and chemical bonds of Au/p-Si(111)-7×7 grown at RT by high-resolution medium energy ion scattering (MEIS) combined with photoelectron spectroscopy (PES) using synchrotron-radiation (SR)-light. The high-resolution MEIS determines the elemental depth profiles with an excellent resolution of ~0.1 nm and quite complementally SR-PES gives information about the electronic properties of the Au/Si system. In such a way, we identify unambiguously the phases together with the chemical bonds of the growing layers including band bending at the hetero-interfaces. The present study is confined to the analysis of Au stacking on the p-Si(111)-7×7 surface at RT for Au coverage up to 13 ML. A small Au deposition on the Si(111)-7×7 surface at higher temperatures grows a variety of super structures on top and the phase diagram is referred to the literatures[21,22].

II. EXPERIMENT

We employed on-axis p-type-Si(111) wafers, which were cut into small pieces, a typical size of 14×14 mm^2. After surface cleaning by a modified Shiraki method[23], the surface was slightly oxidized in a solution of HCl and H_2O_2 (HCl : H_2O_2 : H_2O = 3 : 1 : 1) at 85ºC for 5 min. Then, the sample was introduced into an ultra-high vacuum (UHV) chamber and flashed at 1200 ºC several times by infrared radiation. The surface showed a clear 7×7 pattern, which was observed by reflection high energy electron diffraction (RHEED). A clean surface without any contaminations was confirmed by valence band and MEIS spectra. Au deposition was made at RT with a Knudsen cell at a rate of 0.5 ML/min (1 ML = 0.78×10^{15} atoms/cm^2 : areal density of Si(111)).

MEIS analysis was performed using well collimated 120 keV He^+ and H^+ beams and scattered He^+ and H^+ ions were detected by a toroidal electrostatic analyzer (ESA). The energy resolution is excellent ($\Delta E / E = 9\times10^{-4}$: FWHM) and thus allows elemental depth profiling in a layer-by-layer fashion[24,25]. It is quite crucial for determining the absolute amounts of Au and Si as a function of depth to have reliable data on the charge fractions of He^+ and H^+ emerging from a surface, which are dependent on emerging energy and angle, and elemental species of the surface[26,27].

So, we measured in advance the H^+ and He^+ fractions using a thick Au poly crystal film(~ 4 nm) grown on an SiO_2(4 nm)/Si(001) substrate, whose thickness was measured precisely by a surface-barrier type solid state detector using 2.0 MeV He^+ beams. Another important factor dominating the reliability of MEIS analysis is to measure the integrated beam current accurately. For this purpose, a voltage of +90 V was applied to the sample and the beam current was conducted to ground via an ammeter. In order to avoid the intermixing effect induced by ion irradiation, we shifted the beam position on a sample surface after an integrated beam current of 1 μC. The Au $4f_{5/2,7/2}$ and Si $2p_{1/2,3/2}$ core levels together with valence band spectra were measured at photon energies of 140 and 280 eV by a hemispherical ESA. The incident photon energy was calibrated by primary and the 2nd harmonic waves and the energy resolution was estimated to be 0.05 eV at a pass energy of 2.95 eV. All the experiments were performed *in situ* under UHV conditions ($< 2\times10^{-10}$ Torr).

III. RESULTS AND DISCUSSION

A. PES Analysis

Figure 1 shows the Au $4f_{5/2,7/2}$ core level spectra observed at a photon energy of 140 eV as a function of Au coverage. It is clearly seen that each spectrum is decomposed into two components at an Au coverage above 2.4±0.3 ML. Figure 2 indicates the binding energy (E_B) of Au $4f_{7/2}$ for these two components, as a functions of Au coverage. The peak with a higher E_B value (S_A) originates from an Au-silicide layer on top and that with a lower E_B value (M_A) comes from an underlying Au metallic layer. The component M_A takes a constant E_B value of 84.05±0.05 eV, while the silicide component (S_A) varies with Au coverage from 0.31 to 1.1 ML and becomes constant (84.6±0.05 eV) at an Au coverage above 2.4 ML. In fact, the peak at 84.05 eV was observed for a single crystal Au(111) surface. Such silicide and metallic components were previously reported[15,16] and the E_B values are in good agreement with the above observed ones for Au coverage above 2.4 ML. The stacking sequence of the Au-silcide layer on the metallic one was confirmed by the fact that the intensity ratios of S_A/M_A observed at $h\nu = 140$ eV and at an emission angle of 60° are considerably larger than those at 280 eV and at 0° , respectively. Note that the escape depth of photoelectrons for $h\nu$ = 280 eV is about twice that for $h\nu$ = 140 eV. At an early

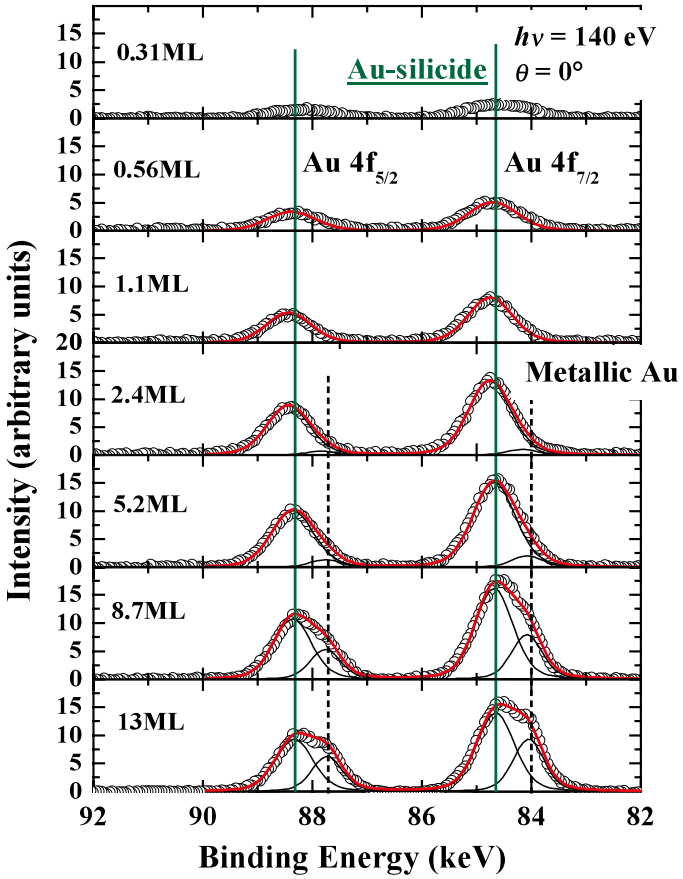

FIG. 1. Au $4f_{5/2,7/2}$ core level spectra observed for varied Au coverage at photon energy of 140 eV under normal emission condition ($\theta = 0^\circ$). Each spectrum is decomposed into two components S_A and M_A for Au coverage above 5.2 ML.

stage of Au deposition from 0.31 to 1.1 ML, only the component S_A is seen, indicating that Au-Si alloying takes place initially. Such an Au-silicidation at Au coverage above 0.31 ML is evidenced by Si 2p core level shifts, as shown later. The intensities of the components S_A and M_A are shown in Fig. 3, as a function of Au coverage. The component S_A is increased rapidly and saturated at Au coverage above 2.4 ML and the component M_A becomes visible clearly at Au coverage of 2.4 ML and then gradually increases with increasing Au coverage.

The Si 2p core level spectra as a function of Au coverage are shown in Fig. 4. The spectra were taken at a photon energy of 140 eV under normal emission condition. The spectrum decomposition for the Si(111)-7×7 surface was reported previously[28] and the 7×7 RHEED pattern disappeared at an Au coverage of 1.1 ML corresponding to

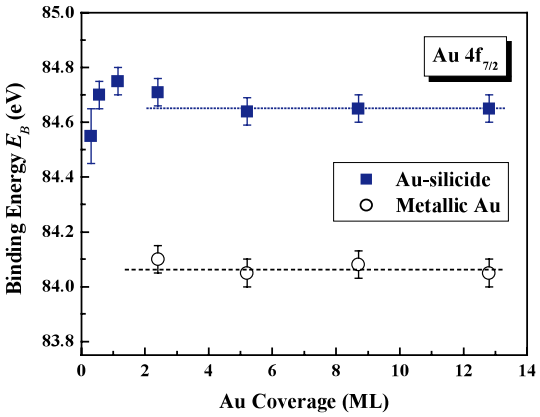

FIG. 2. Binding Energy of Au $4f_{7/2}$ for S_A(silicide) and M_A(metallic) components, as a function of Au coverage. Dashed lines are drawn to guide the eyes.

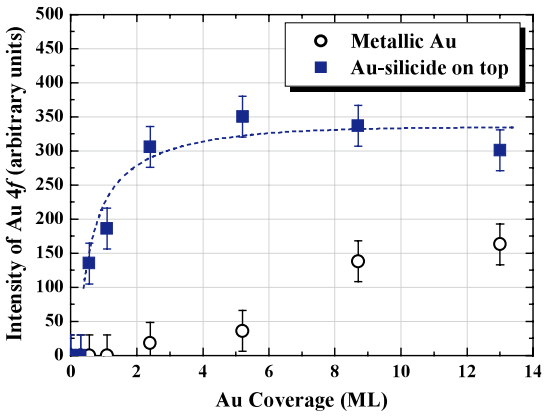

FIG. 3. Au 4f peak intensities of components S_A (open squares) and M_A (full squares) as a function of Au coverage.

0.62 ML of the Au(111) atomic-plane (areal density of Au(111): 1.39×10^{15} atoms/cm^2). The component from the bulk Si (B_S) indicated by the shaded areas in Fig. 4 is identified by the photoelectron intensity dependent on emission angle and photon energy. The component S_S with an E_B value of 99.75±0.05 eV for Si $2p_{3/2}$ peak is dominant at Au coverage above 5.2 ML. The intensity dependent on emission angle and incident photon energy indicates that the component S_S comes from the Si atoms on top and thus originates from a silicide layer, as discussed in the Au 4f spectra. The component M_S takes a constant E_B value of 99.05±0.04 eV independent of Au coverage. What is the origin of the component M_S? As will be shown later in MEIS analysis, we observed Si atoms incorporated in the underlying metallic Au layer for Au coverage above 2.4 ML. This leads to conviction that the M_S originates from Si atoms contained in the intermediate Au layer and do not react with Au atoms. This component with a same E_B value of 99.05 eV is also seen for low Au coverage below 1.1 ML, although the metallic Au 4f level is invisible. This suggests that Si atoms are located near the top of the Si(111) substrate, whose bonds are broken and released from the substrate. In the previous study of Ni deposition on a SiC(0001)-$\sqrt{3}\times\sqrt{3}$ surface at RT[29], we found that Si atoms were incorporated in a Ni-lattice without taking a

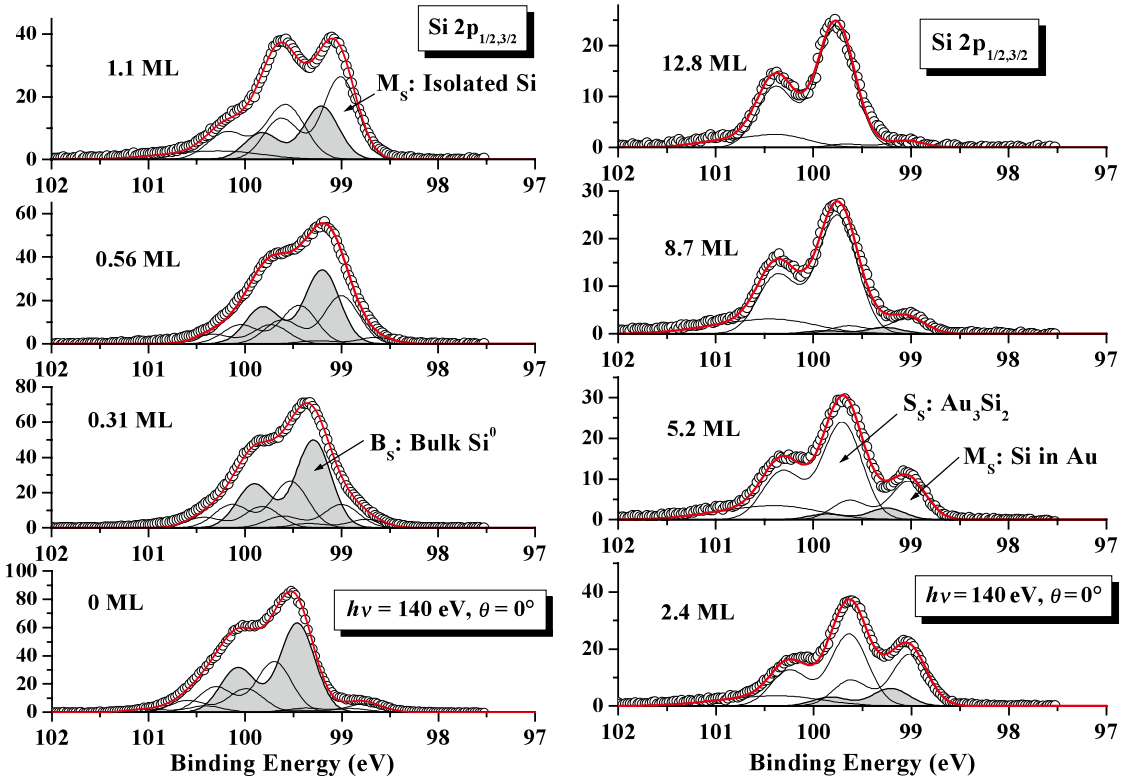

FIG. 4. Si $2p_{1/2,3/2}$ core level spectra observed for varied Au coverage at photon energy of 140 eV under normal emission condition. Grey areas denote bulk component (Si^0).

silicide phase. In the case of Ni deposition on the Si(111)-7×7 surface at RT, a Ni/$NiSi_x$/Si(111) structure is formed and the Ni lattice overlying the Ni-silicide layer contains Si atoms[30].

The E_B values for the above three components are shown in Fig. 5, as a function of Au coverage. The E_B value of B_S (bulk) drops by 0.25 eV by Au deposition of 1.1 ML. This corresponds to disappearance of the 7×7 RHEED pattern, indicating that the band bent downward initially is flattened significantly. Note that the band of the p-Si(111)-7×7 surface bends downward to equalize the Fermi levels of the bulk p-Si(111) and the half-filled surface state band. In the case of n-Si(111)-7×7 surface, the band bends upward by 0.43 eV[31]. Grupp and Ibrahimi[19] determined the Schottky barrier height $\Phi^{(n)}_{SBH}$ to be 0.75±0.04 eV for Au/n-Si(111). If we employ the relation $\Phi^{(n)}_{SBH} + \Phi^{(p)}_{SBH} = 1.12$ eV [32] (band gap), the downward band bending is deduced to be 0.55 eV for p-Si(111)-7×7 (see Fig. 5). According to the data tabulated by Sze[33], the $\Phi^{(p)}_{SBH}$ for Au/p-Si(111) is 0.35 eV, which gives the downward band

bending of 0.53 eV. The E_B value for S_S (Au-silicide) increases significantly with increasing Au coverage up to 5.2 ML and approaches a constant value of 99.80±0.05 eV at Au coverage of 5.2 ML. This is well correlated with the E_B value of Au 4f (see Fig. 2) and indicates that the Au-silicide phase on top is stable for Au coverage above 5.2 ML. It is noteworthy that both Au 4f and Si 2p levels for the top Au-silicide layer take higher binding energy shifts from those for the bulk Au and Si. This suggests a significantly longer bond length of Au-Si compared with the Au-Au and Si-Si bonds, which should lower both core levels.

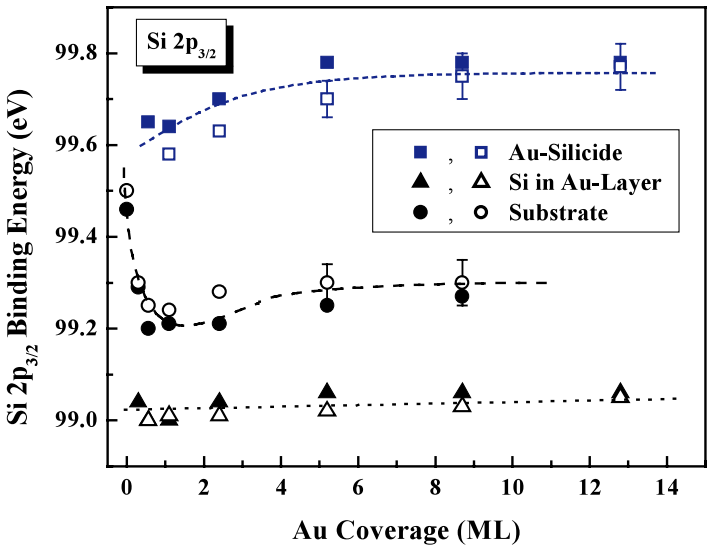

FIG. 5. Binding energy of Si $2p_{3/2}$ for components B_S(circles), S_S(squares), and M_S (triangles) as a function of Au coverage. Open and closed symbols denote incident photon energy of 140 and 280 eV, respectively.

B. MEIS Analysis

The elemental depth profiles for Au-deposited Si(111) were determined by high-resolution MEIS using 120 keV H^+ and He^+ beams. Figures 6(a) - (d) show the MEIS spectra observed for 120 keV He^+ ions incident along the [001]-axis of Si(111) (54.7°) and scattered to 70.5 or 80.0° from Au and Si. The observed spectra were best-fitted by simulated ones assuming three components with different layer thickness for Au coverage above 1.1 ML. Indeed, in order to reproduce the long-tailed or broad spectrum, fluctuation of layer thickness must be taken into account. Here, we employed the stopping power values of $1.0\times S_{Z\text{-}Si}(E)$ and $1.1\times S_{Z\text{-}Au}(E)$ for Si and Au

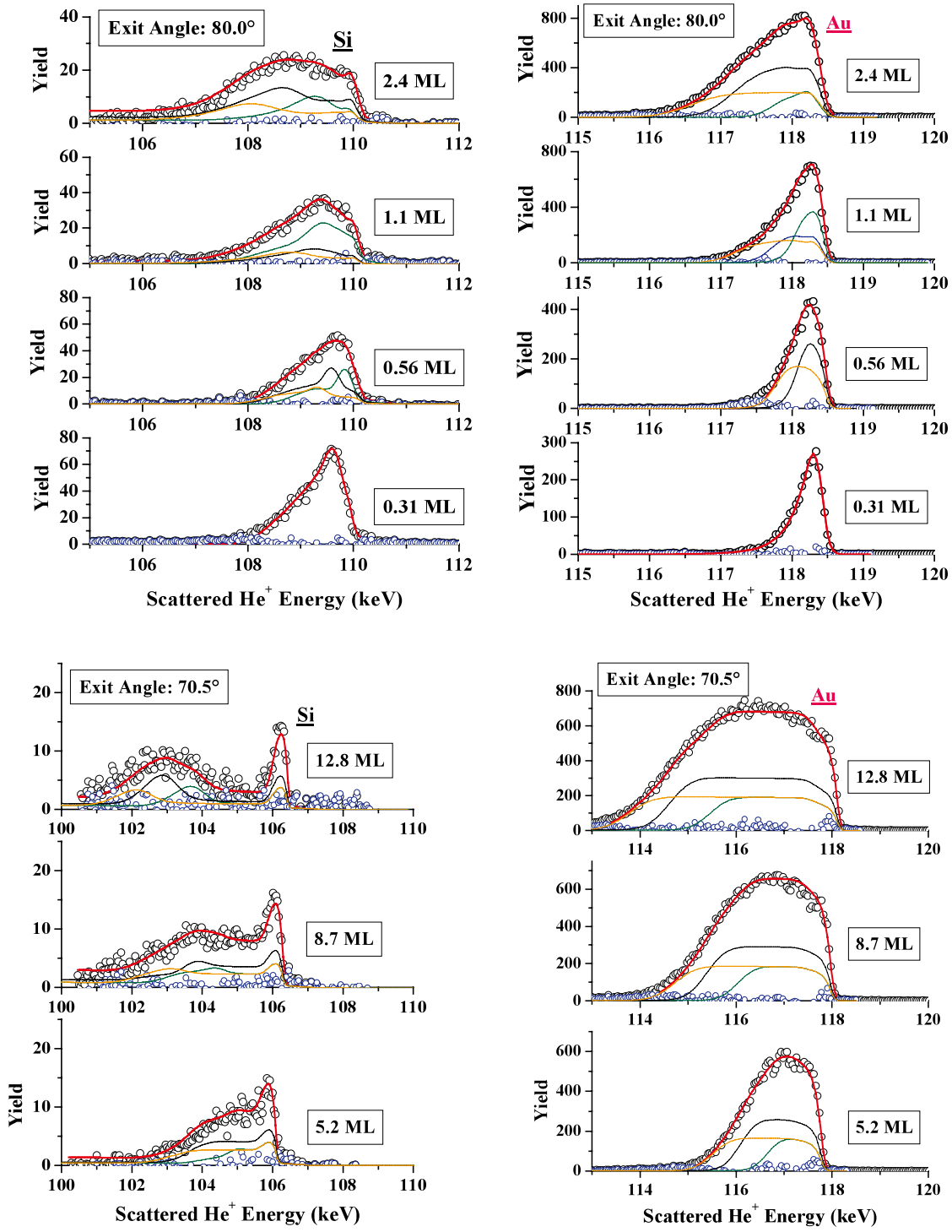

FIG. 6. MEIS spectra observed for 120 keV He^+ ions incident along [100]-axis and scattered to 70.5 and 80.0° from Si ((a) and (c)) and Au ((b) and (d)) with respect to surface normal. Simulated spectra (total: thick solid curves) are best-fitted to observed ones (circles) assuming appropriate layer thickness, elemental compositions and thickness fluctuations. Blue circles denote the difference spectrum obtained by subtracting the best-fit total spectrum from the observed one.

For Au coverage above 5.2 ML, the surface consists of Au_3Si_2 (1.5×10^{15} atoms/cm^2) layer on top and of an underlying Au layer containing Si with thickness fluctuation which obeys a Poisson distribution. Representatively, we take three points, center (45.2 %) and its both sides apart by the standard deviation (27.4 %).

($S_Z(E)$: Ziegler's stopping powers[34]), respectively. The He^+ fractions for the scattering components from top Au and Si atoms (non-equilibrium) are 45 and 46 % and those (equilibrium) from underlying Au and Si are 41 and 43 %, respectively[27]. These stopping powers and charge fractions were determined in advance using Au(~4 nm)/SiO_2/Si(111) and Si(~4 nm)/HOPG (highly ordered pyrolytic graphite). In addition, the scattering component from Au in a top-layer has an asymmetric nature due to inner shell excitations, which is expressed by an exponentially modified Gaussian shape proposed by Grande et al.[35].

For Au coverage of 0.31 ML, assumption of two-dimensional (2D) islands of Au with one atomic-layer height on the Si substrate reproduces well the observed MEIS spectrum. The height of Au atoms deposited is compatible with that of the top Si(111) plane. According to an X-ray standing wave analysis[36], the Au atoms are distributed almost randomly in the lateral plane and embedded in a depth of 0.03 and 0.09 nm from the top Si-plane at Au coverage of 0.3 and 0.4 ML, respectively. However, judging from the slopes of the front edges for the MEIS spectra from Au and Si atoms, the Au atoms take a position in height compatible with the top Si-plane or slightly upward, although the height may be fluctuated significantly. In the local Au-deposited region, the 7×7 structure is broken, because the 7×7 RHEED pattern disappeared at Au coverage of 1.1 ML. The Au 4f spectrum (see Figs. 1 and 2) observed at Au coverage of 0.31 ML shows a broad peak with an E_B value shifted significantly to the higher energy side, indicating Au-silicide growth. Such a higher E_B shift at a small Au coverage was reported previously[12,13,18]. Ghose et al.[37] analyzed the Si(111)-7×7 surface deposited with Au (0.06 to 0.18 ML) at RT by surface X-ray diffraction combined with first principles calculation based on the density functional theory (DFT) and concluded formation of a metastable (2D) nanocluster on the faulted halves of the unit cell. On the other hand, Liu et al.[38] predicted based on DFT calculations using the Gaussian 98 program package that Au atoms take the on top site

and a strong interaction between Au atoms and the dangling bonds of surface Si atoms. The present MEIS coupled with PES analysis also suggests growth of some metastable Au-silicide phase at Au coverage of 0.31 ML.

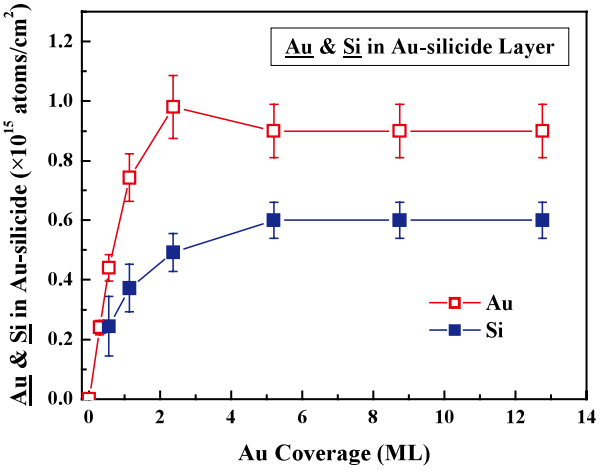

FIG. 7. Absolute amounts of Au (full squares) and Si(open squares) incorporated in the Au-silicide layer on top as a function of Au coverage, which were determined by high-resolution MEIS.

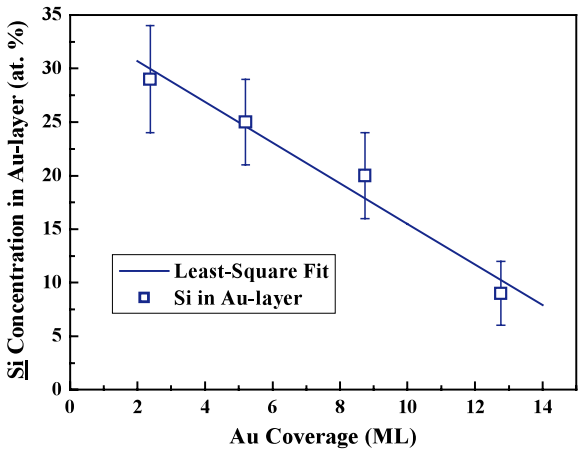

FIG. 8. Si concentration (at. %) in Au-layer determined by MEIS, as a function of Au coverage. Si atoms isolated from Si(111) but remaining at Au/Si interface are expected. Solid line indicates linear least-square fitting.

For Au coverage of 0.56 ML, the MEIS spectrum is reproduced well assuming two kinds of domains of Au_2Si (average) with thickness of 0.78×10^{15} atoms/cm^2(areal occupation ratio: σ = 45 %) and $2\times0.78\times10^{15}$ atoms/cm^2(σ = 25 %). This means a significant fluctuation of the Au-silicide layer thickness. At an Au coverage of 1.1 ML, the surface is covered completely with an Au-silicide layer with an average composition of Au_2Si. The observed MEIS spectrum is fitted well by taking account of fluctuation of the layer thickness. Here, we assume three kinds of domains with thickness of 0.78×10^{15}(σ = 50 %), $2\times0.78\times10^{15}$(σ = 30 %), and $3\times0.78\times10^{15}$ atoms/cm^2(σ = 20 %). The fact that the average composition of Au_2Si does not change is responsible for balance between deposited Au atoms and the isolated Si atoms diffused into the Au layer. Increase in Au coverage to 2.4 ML results in an average elemental composition of $Au_{2.2}Si$.

For Au coverage above 5.2 ML, the MEIS analysis reveals unambiguously growth

of a structure of Au_3Si_2/Au(Si)/Si(111). The surface peak clearly seen in the MEIS spectrum from Si atoms comes from the Au_3Si_2 layer on top (see Fig. 6(c)). Figure 7 shows the absolute amounts of Au and Si in the top Au-silicide layer determined by MEIS. For small Au coverage below 1.1 ML, some silicide phases with average composition of Au_2Si seem to grow but a single phase or not and the elemental composition are uncertain, as mentioned above. As can be seen from Figs. 2 and 7, a precursor state of the Au_3Si_2 phase is already formed at Au coverage of 2.4 ML. It is clearly seen that the Au_3Si_2 phase grows and the thickness of the Au_3Si_2 layer is saturated with $1.50\pm0.15\times10^{15}$ atoms/cm^2 (~2 atomic layers) at an Au coverage of 5.2 ML. The thickness and elemental composition remain constant up to an Au coverage of 12.8 ML. This is consistent with the binding energy shifts of Au $4f_{7/2}$ and Si $2p_{3/2}$ as a function of Au coverage (Figs. 2 and 5). Deposited Au atoms penetrate through the Au_3Si_2 layer to grow the non-reacted Au layer above the Si(111) substrate. The Si atoms separated from the Si(111) substrate but remaining near the Au(Si)/Si(111) interface are then solute into the metallic Au layer. The concentration of Si contained in the metallic Au layer is almost homogeneous and decreases linearly with increase in Au coverage, as shown in Fig. 8. The Si atoms diffused into the Au layer are blocked by the Au_3Si_2 layer and do not segregate on the surface. Indeed, such a dilution of Si concentration weakens the photoelectron intensity of Si 2p (M_S) from the Si atoms incorporated in the Au layer (see Fig. 4). The homogeneous distribution of Si atoms in the Au layer suggests a long enough diffusion length compared with the Au thickness for Si diffusion in Au layers at RT. The linear decrease in the Si concentration leads to a quadratic increase in total amount of Si solute into the Au layer. From the least-square fit to the observed Si concentration indicated in Fig. 8, the number of Si atoms solute into the Au layer is deduced to be saturated with 1.23×10^{15} atoms/cm^2 at Au coverage ~10 ML (see Fig. 9). The deviation from the above estimate seen at Au coverage of 12.8 ML is due to the fact that the accuracy of the Si content in the Au layer is degraded with decreasing the Si concentration in MEIS analysis. The total amount of Si atoms contained in the Au-silicide and metallic Au layer is saturated at 2.34 ML(1.83×10^{15} atoms/cm^2), coinciding with the number of Si atoms constructing the 7×7 structure ($1.63\pm0.20\times10^{15}$ atoms/cm^2) within an experimental uncertainty.

Concerning the Au-silicide phase, the Au_3Si compound has been expected from the

eutectic point of the Au-Si binary phase diagram[15,16]. We must note, however, that this phase can be obtained by quenching from a high temperature to RT and application of the phase diagram is limited to bulk materials, not to such an ultra-thin (~2 atomic layers) Au-silicide layer[16]. The Au_3Si_2 phase may be also metastable and grow only under the constraint of Au deposition at a slow rate (< 1 ML/min) on the clean Si(111)-7×7 surface at RT. There are quite similar reports so far. Kim et al.[20] reported the ratio of Au/Si about 1.5 derived by electron-induced Auger electron spectroscopy. Low energy ion scattering analysis[18] also estimated the Au concentration to be about 60%.

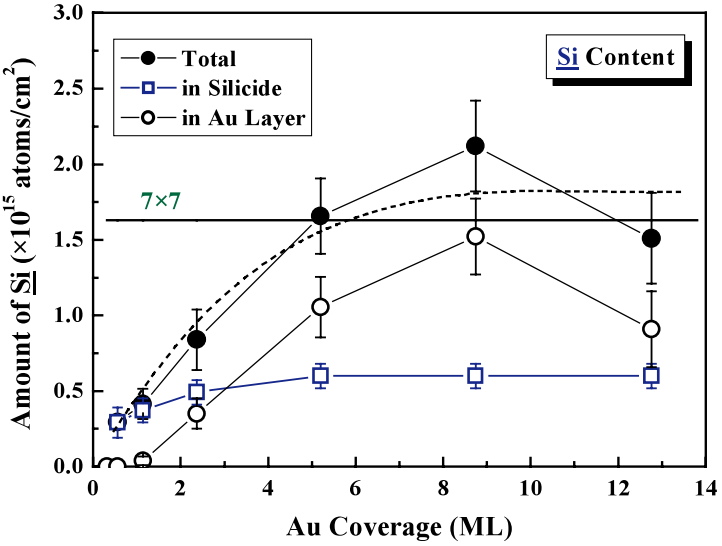

FIG. 9. Total (full circles) and fractions of Si atoms contained in Au-silicide (open squares) and in metallic Au-layer (open circles). Si atoms separated from Si(111) substrate but remaining at Au/Si interface are excepted from those contained in Au-layer. Solid line indicates the amount of Si atoms making the 7×7 reconstruction (1.63×10^{15} atoms/cm^2). Quadratic curve (dashed) saturated at Au coverage of ~10 ML denotes the number of Si atoms contained in Au-silicide and Au layers, which is estimated from least-square fitting of Si concentration in Au layer.

From the discussion presented above, we can see the dynamical process for Au deposition on the clean Si(111)-7×7 surface. It is interesting to point out here that the number of Si atoms to form the Au_3Si_2 (1.5×10^{15} atoms/cm^2) layer is ~3/4 ML, which coincides well with 36/49 ML, the number of the adatoms and rest atoms with dangling bonds together with the dimers located at the edge of the 7×7 unit mesh. They (group

A) are first attacked by Au atoms, leading to Si-Si bond breaking and formation of Au-silicides at a small Au coverage. In fact, the DFT calculations predicted a strong interaction between Au and the dangling bonds of surface Si atoms. At Au coverage of 2.4 ML the Au_3Si_2 domains may partly grow or some precursor state may emerge. Here, an elemental question arises why not all the Si atoms released from the Si(111)-7×7 surface are consumed to form the Au_3Si_2 layer. A probable interpretation is that bond breaking of the underlying Si atoms comprising the residual 7×7 reconstruction (group B) is substantially delayed in other word the bonds are not easily broken compared with the group A and thus the Au atoms arriving at the Au-silicide/Si(111) interface coalesce to form small Au clusters rather than react with the Si atoms. After formation of Au clusters at the interface, the Si atoms released from the bulk-truncated Si(111) plane diffuse via grain boundaries of Au clusters. This is the reason why the surface takes the Au_3Si_2 layer on top with thickness of 1.5×10^{15} atoms/cm^2 and the underlying Au layer contains Si atoms without alloying. The growth process for the Au/Si(111) system is illustrated in Fig. 10.

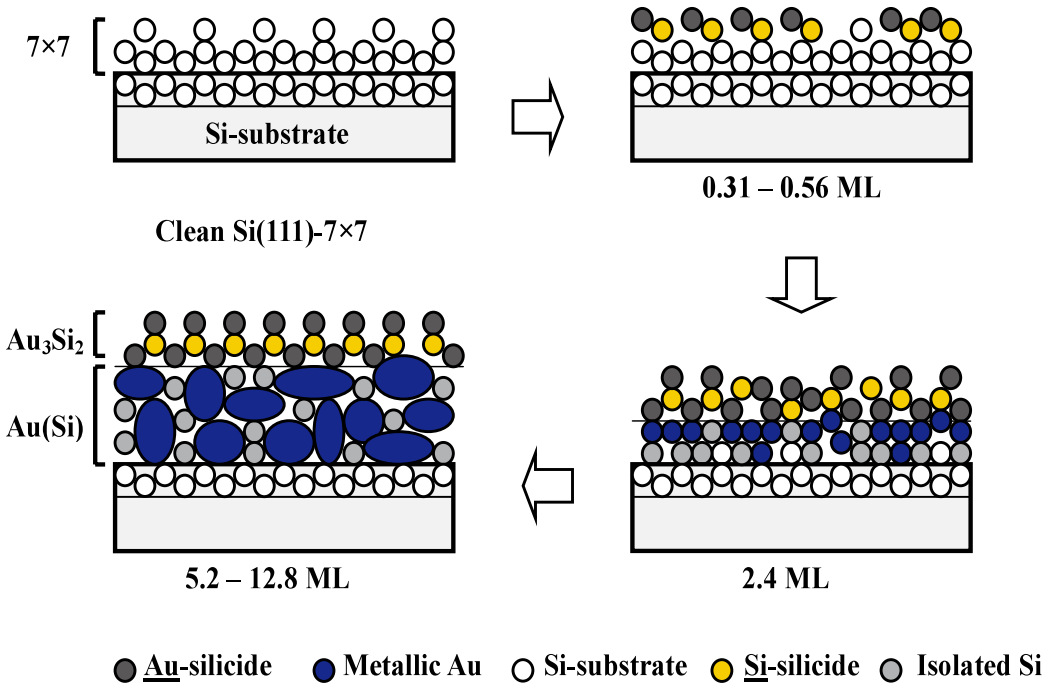

FIG. 10. Growth process for Au deposition on Si(111)-7×7 at RT. White, orange, and grey circles denote Si atoms of substrate, Au-silicde, and separated from substrate, respectively. Black circles indicate Au atoms of silicide and blue symbol means metallic Au.

IV. CONCLUSION

We analyzed both the phase and electronic structures of Au layers grown on the clean p-Si(111)-7×7 surface at RT by high-resolution MEIS combined with PES using SR-light. It is found that an Au-silicide layer is formed at Au coverage of 0.31 ML which is confirmed by observation of Au 4f core level spectra. For Au coverage above 5.2 ML the surface consists of a stable Au_3Si_2 layer with thickness of 1.5×10^{15} atoms/cm^2 on top and an underlying metallic Au layer which contains Si atoms probably diffused in the boundaries of fine Au clusters. In this regard, we observed two components for Au 4f (Au-silicide and metallic) and three components for Si 2p (bulk, Au-silicide, and incorporated in an Au layer) spectra. The E_B values of Au $4f_{7/2}$ observed are 84.05±0.05 eV (M_A: metallic Au) and 84.60±0.05 eV (S_A: Au-silicide) and those of Si $2p_{3/2}$ are determined to be (i) 99.05±0.04 (M_S: incorporated in Au layer), (ii) 99.30±0.04 (B_S: bulk Si), and (iii) 99.75±0.05 (S_S: Au-silicide) eV. The stacking sequence of an Au-silicide layer on a metallic Au layer which grows on Si(111) is confirmed by the intensity ratio ($S_{A(S)}/M_{A(S)}$) of the silicide component to metallic one dependent on incident photon energy (140, 280 eV) and emission angle (0° and 60°). With increasing Au coverage from 5.2 to 12.8 ML thickness of the Au_3Si_2 layer does not change, while thickness of the underlying Au layer increases and the concentration of Si in the Au layer decreases linearly. Total amount of Si atoms contained in the Au_3Si_2 and underlying Au layers coincides with the number of Si atoms constituting the 7×7 reconstruction. The number of Si atoms forming the Au_3Si_2 layer is determined to be 0.6×10^{15} atoms/cm^2 (~3/4 ML), which corresponds to that (36/49 ML) of Si adatoms and rest atoms with dangling bonds plus dimers located at the edge of the 7×7 unit cell.

The growing process for Au on the Si(111)-7×7 surface is speculated as follows: The Si adatoms and rest atoms plus dimers are first attacked by Au atoms, leading to Si-Si bond breaking and formation of Au-silicides at a small Au coverage. At an Au coverage of 2.4 ML the Au_3Si_2 domains may partly grow or its precursor may emerge. Bond breaking of the underlying Si atoms comprising the residual 7×7 reconstruction is substantially delayed and thus the Au atoms arriving at the Au-silicide/Si(111) interface coalesce to form small Au clusters before reacting with the Si atoms. After formation of Au clusters at the interface, the Si atoms released from the bulk-truncated Si(111) plane diffuse into grain boundaries of Au clusters. This is the reason why the surface

takes the Au_3Si_2 layer on top with a constant thickness of 1.5×10^{15} atoms/cm^2 and the underlying Au layer contains Si atoms without alloying.

Acknowledgments

We appreciate Prof. H. Namba for his many efforts to maintain the BL-8. Thanks are also due to our colleagues, Dr. T. Nishimura and Dr. T. Okazawa for valuable discussion and useful comments. This work was partly supported by Japan Science and Technology Agency, JST, CREST.

References

[1] T. Narusawa, S. Komiya, and A. Hiraki, Appl. Phys. Lett. **22** (1973) 389.

[2] L. Braicovich, C.M. Garner, P.R. Skeath, C.Y. Su, P.W. Chye, I. Lindau, and W.E. Spicer, Phys. Rev. **B 20** (1979) 5131.

[3] A. Hiraki, Surf. Sci. Rep. **3** (1983) 355.

[4] C. Calandra, O. Bisi, and G. Ottabiani, Surf. Sci. Rept. **4** (1985) 271.

[5] A. Hiraki, E. Lugujjo, and J.W. Mayer, J. Appl. Phys. **43**,(1972) 3643.

[6] M. Haruta, T. Kobayashi, H. Sano, and N. Yamada, Chem. Lett. **2** (1987) 405.

[7] M. Haruta, Catal. Today **36**,(1997) 153.

[8] M. Valden, X. Lai, and D.W. Goodman, Science **281** (1998) 1647.

[9] K. Okuno, T. Ito, M. Iwami, and A. Hiraki, Solid State Commun. **34**,(1980) 493.

[10] T. Narusawa, W.M. Gibson, and A. Hiraki, Phys. Rev. **B 24**, (1981) 4835.

[11] G. Le Lay, Surf. Sci. **132** (1983) 169.

[12] H. Dallaporta and A. Cros, Surf. Sci. **178** (1986) 64.

[13] M. Iwami, T. Terada, H. Tochihara, M. Kubota, and Y. Murata, Surf. Sci. **194** (1988) 115.

[14] B. Vogt, P. Stoppmanns, B. Schmiedeskamp, and U. Heinzmann, Appl. Phys. **A 52**,(1991) 323.

[15] S.L. Molodtsov, C. Laubschat, A.M. Shikin, and V.K. Adamchuk, Surf. Sci. **269/270** (1992) 988.

[16] J.-J. Yeh, J. Hwang, K. Bertness, D.J. Friedman, R. Cao, and I. Lindau, Phys. Rev. Lett. **70** (1993) 3768.

[17] E. Landree, D. Grozea, C. Collazo-Davila, and L.D. Marks, Phys. Rev. **B 55** (1997) 7910.

[18] W.C.A.N. Ceelen, B. Moest, M. de Ridder, L.J. van IJzendoom, A.W. Denier van der Gon, and H.H. Brongersma, Appl. Surf. Sci. **134**,(1998) 87.

[19] C. Grupp and A. Taleb-Ibrahimi, Phys. Rev. **B 57** (1998) 6258.

[20] J.H. Kim, G. Yang, S. Yang, and A.H. Weiss, Surf. Sci. **475** (2001) 37.

[21] K. Oura, M. Katayama, F. Shoji, and T. Hanawa, Phys. Rev. Lett. **55** (1985) 1486.

[22] T. Nagao, S. Hasegawa, K. Tsuchie, S. Ino, C. Voges, G. Klos, H. Pfnür, and M. Henzler, Phys. Rev. **B 57** (1998) 10100.

[23] T. Nishimura, Y. Hoshino, H. Namba, and Y. Kido, Surf. Sci. **461**,(2000) 146.

[24] T. Nishimura, A. Ikeda, and Y. Kido, Rev. Sci. Instrum. **69** (1998) 1671.

[25] Y. Kido, T. Nishimura, Y. Hoshino, and H. Namba, Nucl. Instrum. Methods **B161-163**,(2000) 371.

[26] Y. Kido, F. Fukumura, and T. Nishimura, Phys. Rev. Lett. **82** (1999) 3352.

[27] T. Okazawa, K. Shibuya, T. Nishimura, and Y. Kido, Nucl. Instrum. Methods **B 256**,(2007) 1.

[28] T. Nishimura, Y. Hoshino, H. Namba, Y. Kido, Surf. Sci. **461**, 146 (2000).

[29] Y. Hoshino, S. Matsumoto, and Y. Kido, Phys. Rev. **B 69**, 155303 (2004).

[30] T. Nishimura, J. Takeda, Y. Asami, Y. Hoshino, and Y. Kido, Surf. Sci. **588** (2005) 71.

[31] S. Tanuma, T. Shiratori, T. Kimura, K. Goto, S. Ichimura, and C.J. Powell, Surf. and Int. Analysis **37** (2005) 833.

[32] C.K. Karlsson, E. Landmark, L.S.O. Johansson, U.O. Karlsson, and R.I.G. Uhrberg, Phys. Rev. **B 41** (1990) 1521.

[33] S.M. Sze, *Physics of Semiconductor Devices*, 2nd ed. (Wiley, New York, 1981)

[34] J.F. Ziegler, J.P. Biersack, and W. Littmark, *The Stopping and Range of Ions in Matter* (Pergamon, New York, 1985).

[35] P.L. Grande, A. Hentz, R.P. Pezzi, I.J.R. Baumvol, G. Schiwietz, Nucl. Instrum. Methods **B 256** (2007) 92.

[36] S.M. Durbin, L.E. Berman, B.W. Batterman, and J.M. Blakely, Phys. Rev. **B 33** (1986) 4402.

[37] S.K. Ghose, P.A. Bennett, and I.K. Robinson, Phys. Rev. **B 71** (2005) 073407.

[38] Y. Liu, M. Li, and Y. Suo, Surf. Sci. **600**,(2006) 5117.